Journal of Molecular Liquids 367 (2022) 120446

Contents lists available at ScienceDirect

Journal of Molecular Liquids

journal homepage: www.elsevier.com/locate/molliq

Physicochemical characterisation of graphene-ammonium lactate ionic liquid nanofluid

Pablo Manuel Martínez-Rubio, María Dolores Avilés, Joaquín Arias-Pardilla, Francisco José Carrión-Vilches, José Sanes, María Dolores Bermúdez, Ramón Pamies *

Grupo de Ciencia de Materiales e Ingeniería Metalúrgica, Universidad Politécnica de Cartagena, Campus de la Muralla del Mar, 30202-Cartagena, Spain

ARTICLE INFO

Article history:
Received 10 June 2022
Revised 2 September 2022
Accepted 20 September 2022
Available online 26 September 2022

Keywords:
Graphene
Ionic liquids
Rheology
Conductivity

ABSTRACT

A new series of nanofluids based on graphene dispersed in 2-hydroxyethylammonium lactate (ML) ionic liquid was developed. Concentrations of 0.1, 0.5 and 1 wt% of graphene were studied and these dispersions were stable after 2 months. Raman spectra showed a strong interaction between ML and graphene. The effect of the concentration of graphene and temperature on the viscoelastic behaviour and conductivity of the nanofluids was studied. An unexpected decrease in the viscosity was found with a low concentration of graphene due to the suppression of hydrogen bonding of the ionic liquid. Shear thinning effects appeared with higher concentrations of graphene and Ostwald and Herschel-Bulkley equations were used to describe the steady-state viscosity results. Creep-recovery tests were also performed, and the data were fitted to a complex Burgers model for the nanofluid with 1 wt% of graphene, with a 47 % of elastic response. The complexity of the model was related to the presence of different molecular arrangements in the nanofluid. An enhancement of the conductivity was observed with increasing values of the graphene concentration. The effect of temperature on viscosity and electrical conductivity was successfully modelled by using both Vogel-Fulcher-Tammann and Power Law equations. Electrochemical characterisation at room temperature was also carried out, finding an irreversible oxidation at 1 V only for the highest concentration (1 wt%). The concentration of percolation was estimated in the range of 0.5 to 1 wt% of graphene.

1. Introduction

Since graphene (G) was isolated in 2004 by Geim and Novoselov [1], this carbon allotrope has attracted the interest of the scientific community due to its unique properties [2–5]. Graphene is a one-atom-thick planar sheet, composed of carbon atoms displayed into a honeycomb lattice. Graphenic structures consist of multi-layered sheets, and it is considered that G can be found in different arrangements, such as graphene monolayers, graphene nanosheets and graphene nanoplatelets [6]. This nanomaterial and its derivatives present applications in many different technological fields such as energy storage [7], biomedicine [8], sensors [9] and coatings [10], among others.

In recent years, the development and design of new ionic liquids (ILs) has raised due to their increasing technical and scientific purposes [11–13]. Ionic liquids are molten salts at room temperature composed of an organic cation and an anion which can be either organic or inorganic. ILs are commonly divided into two categories: protic (PILs) and aprotic (AILs). PILs are the product of a Brønsted acid-base reaction [14,15]. Therefore, PILs are easily synthesized in a one-pot reaction without the formation of by-products, i.e., in a more economical and environmentally sustainable method. The multiple combinations of the different types of cations and anions give rise to an enormous amount of tunable properties and applications. One of these applications is the usage as dispersant media for different types of nanomaterials [16,17]. In the case of graphene, ionic liquids have proven to form stable nanofluids owing to the strong van der Waals interactions and to the hindrance of self-assembly of the plates [18,19]. The advantages of using ILs as the continuous phase of the nanodispersion are wider operating temperature ranges, higher thermal and chemical stability, and negligible vapour pressure, among others [20–24].

The rheological properties of nanofluids exhibit a complex performance [25,26]. Transitions from ordered to disordered states are the most common explanation for their non-Newtonian behaviour. The rheological experimental data along with *in silico* studies allow

* Corresponding author.
E-mail address: ramon.pamies@upct.es (R. Pamies).

https://doi.org/10.1016/j.molliq.2022.120446
0167-7322/

Nomenclature

A	pre-exponential factor in Ostwald-de-Waale and Herschel-Bulkley models	T_x	threshold temperature
A_i	pre-exponential factor in VTF model for viscosity and conductivity	Γ	exponent in power law
D	strength index	η_o	viscosity asymptote value
E_{KV}	elastic element in Kelvin-Voigt model	η_M	viscous element in Maxwell model
E_M	elastic element in Maxwell model	η_{KV}	viscous element in Kelvin-Voigt model
K_i	thermal sensitivity of viscosity and conductivity	λ	retardation time
n	exponential power in Ostwald-de-Waale and Herschel-Bulkley models	μ_o	relaxation time
T_o	theoretical temperature at which the fluid starts to flow	σ_o	conductivity asymptote value
		τ_o	yield stress

the exploration of interactions prevailing in the nanofluid systems [27]. Ionic liquids are able to stabilize filler nanoparticles by ionic solvation of the surface and, therefore, these structural changes are reflected in their rheological properties [28]. By increasing the concentration of nanoparticles in the nanofluids, the non-Newtonian behaviour becomes stronger and the optimum weight fraction of the nanomaterials can be evaluated from the rheological data [29]. Consequently, rheology is a powerful tool to understand the influence of various physical and chemical factors and applications of nanofluids [30–32] such as lubrication [33] or energy storage [34].

In this work, we have studied the rheological behaviour of a nanofluid composed of graphene dispersed in PIL 2-hydroxyethylammonium lactate (ML) salt synthesized by acid-base neutralization. This ionic liquid is known for its biodegradability and low toxicity [35] in order to use eco-friendly nanofluids. Raman and FT-IR spectroscopy have been utilised to evaluate structural changes in graphene when it is dispersed in ML. Concentrations of 0.1, 0.5 and 1 wt% of graphene were used in this study. The influence of the concentration of graphene on the viscosity of ML has been explored, and Ostwald and Herschel-Bulkley models have been applied to assess the non-Newtonian behaviour of the nanofluids. A creep-recovery test has been carried out and the data have been fitted to a complex Burgers model, firstly used for this kind of graphene-ionic liquid nanofluids. The temperature effect on the viscosity and conductivity has been also evaluated by means of the Vogel-Fulcher-Tammann and Power Law equations to evaluate the strengthening effect of graphene. Finally, cyclic voltammograms have been carried out in order to evaluate the electrochemical response. To the best of our knowledge, this cyclic voltammetry has not been previously conducted with this kind of graphene-PIL nanofluid. Combining the electrochemical and viscoelastic studies, we were able to estimate the concentration of percolation.

2. Materials and methods

2.1. Materials

2-hydroxyethylamine was purchased from Sigma-Aldrich, with 99 % purity, while lactic acid was obtained from Sigma-Aldrich, with purity greater than 85 %. These components were used as received. The reaction is a simple Brønsted acid-base neutralization, producing a 2-hydroxyethylammonium lactate salt as it is depicted in Scheme 1. The product was prepared following the methodology described in previous works [36,37].

Graphene was purchased from Iolitec GmbH, Germany (1–10 layers; purity > 99 wt%). Full characterisation of the nanomaterial was previously carried out in our earlier works [26,38,39]. The dispersions of graphene in ML were prepared by addition of 0.1, 0.5, and 1 wt% proportions of graphene to the ionic liquid. These values were chosen in order to observe remarkable effects on the physicochemical properties [40,41]. The materials were weighed (approximately 3 g of mixture) and mixed in an agate mortar and manually blended for 10 min and then sonicated with a Labsonic M from Sartorius (probe with a diameter of 0.5 mm) for 30 min under 1 cycle and a power of 100 W. This sonication was performed in double boiler at 30 °C as it is described in our previous works [42,43]. The resulting dispersions are shown in Fig. 1a and 1b. No phase separation was seen after more than 2 months of observation (Fig. 1b).

3. Methods

The structural characterisation of the samples was carried out using a Fourier Transform Infrared (FTIR) spectrometer Thermo Nicolet 5700 and a Confocal Raman Microscope Witec Alpha 3000. Viscosity measurements of pure ML and its dispersions with graphene were performed with an AR-G2 rotational rheometer from TA Instruments (New Castle, Delaware, USA). A plate-plate configuration was used with a rotational plate of 40 mm. The temperature was controlled by a Peltier system with an accuracy of 0.1 °C. Three different kinds of tests were carried out to investigate the effect of different concentrations of graphene on the viscoelastic behaviour of ML. Firstly, a study of the steady-state viscosity by increasing the shear rate to 500 s^{-1} at a constant temperature set to 25 °C. Secondly, the temperature dependence of the samples was examined in the range of 20–120 °C executing temperature ramps at a constant shear rate of 50 s^{-1}. The linear viscoelastic region was determined with values in the range of 0.1 to 3 Pa. Creep-recovery tests were also accomplished under linear viscoelastic conditions. The applied stress was set to 1 Pa and the creep and recovery times were 5 min in both cases. All the tests were carried out at least 3 times and data are presented as average values with error bars calculated from the standard deviation. Electrical conductivity measurements were performed with Cyberscan COND600 conductivity meter from Eutech Instruments in combination with a refrigerated heating circulating bath LT Ecocool from Grant Instruments (United Kingdom). Using Labwise control software, 4 consecutive heating and cooling cycles between 20 and 90 °C at a rate of 2 °C/min were performed acquiring the electrical conductivity value every degree. The electrical conductivity values shown are the average of these 4 cycles. Cyclic voltammetry tests were carried out using a Biologic SP-300 potentiostat. Platinum electrodes were used as working, counter and reference electrodes. This pseudoreference electrode was selected because it avoids any water contamination. Potential sweeps have been performed from −1 V to 4 V at a sweep speed of 10 mVs^{-1}.

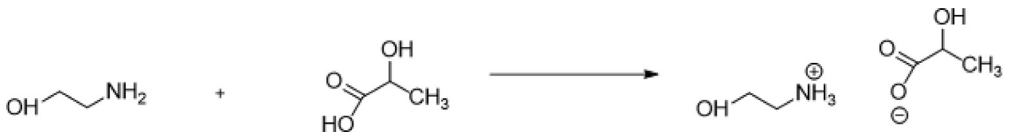

Scheme 1. Synthesis of 2-hydroxyethylammonium lactate (ML) from 2-hydroxyethylamine and lactic acid.

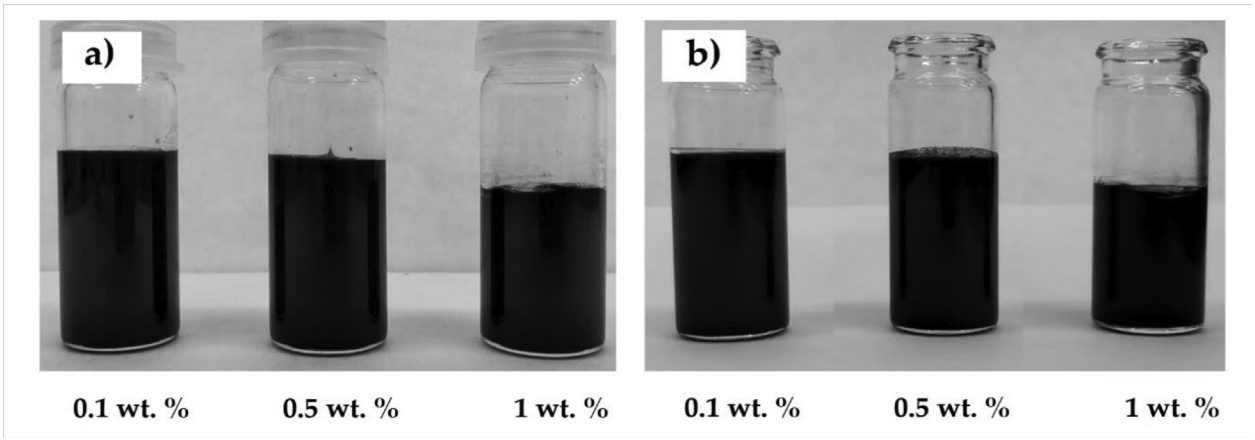

Fig. 1. Graphene-ML dispersions with 0.1 wt%, 0.5 wt% and 1 wt% graphene. a) Freshly prepared and b) after 2 months.

4. Results and discussion

4.1. Raman and FT-IR spectroscopy

The Raman and FT-IR spectra of the newly synthesized ionic liquid are shown in Fig. 2a, and these data are collected in Table 1 with the corresponding assignments. According to previous literature [44], we assigned the Raman peaks at 550, 859, 1473 and the band at circa 3000 cm^{-1} to the ωCOO⁻, υC-COO⁻, δCH_3 and υCH_3/υCH of the lactate, respectively. In the case of the 2-hydroxylammonium cation, the modes of δCH_2, υCN were seen at 865 cm^{-1}, δCH at 1473 cm^{-1}, δNH at 1642 cm^{-1}, and the bands from 2900 to 3000 cm^{-1} are in agreement with υCH_2, υNH_2 [45]. Thus, an overlapping of some bands of the anion and the cation was observed and the assignment was uncertain. A similar situation appeared in the FT-IR spectra. According to Simijonović et al.

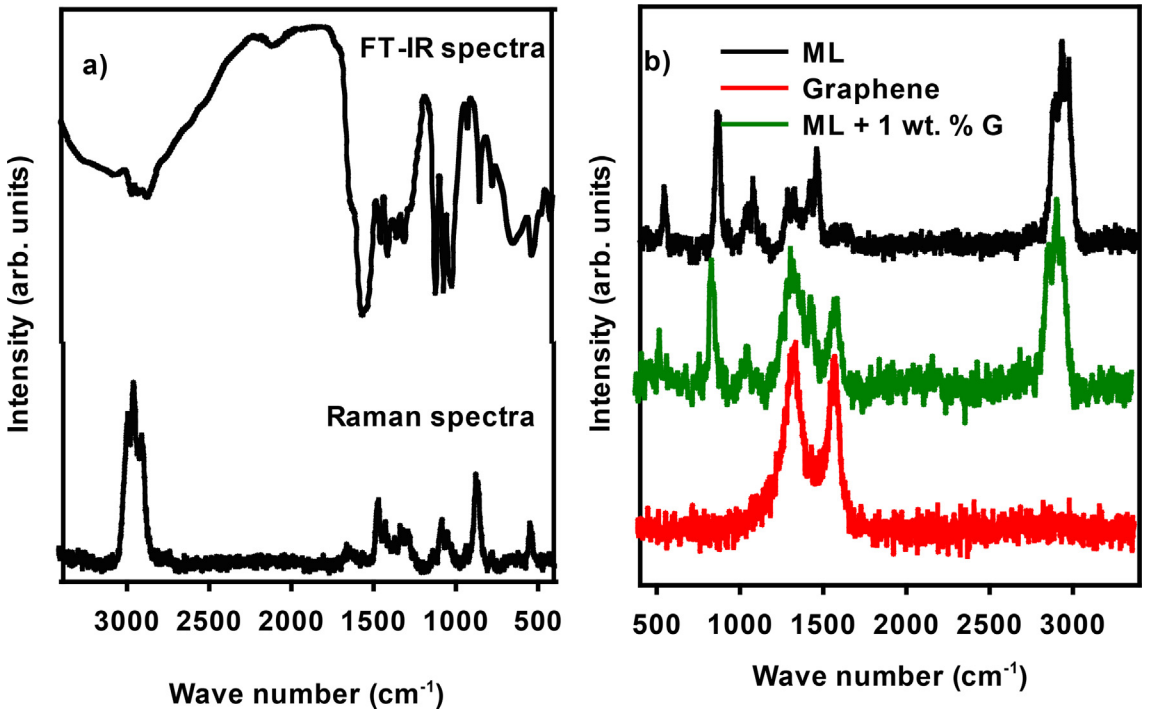

Fig. 2. a) Raman and FT-IR spectra of ML. b) Comparison of the Raman spectra for pure ML and graphene with the 1 wt% dispersion.

Table 1
Raman and FT-IR assignments for ML.

Raman peak (cm^{-1})	Assignment	FT-IR peak (cm^{-1})	Assignment
550	ωCOO^-	1410	υCOO^-
859	$\upsilon C\text{-}COO^-$	1450	$\delta N\text{-}H$
865	δCH_2, υCN	1560	υCOO^-
1052	$\upsilon C\text{-}CH_3$	2930	υCH
1080	υCO	2970	υCH
1288, 1336	δCH		
1368	δCH_3		
1423	υCOO^-		
1473	δCH_3, δCH		
1642	δNH		
2899	υCH_3, υCH_2, υCH		
2948	υCH_3, υCH_2, υCH		
2983	υCH_3, υCH, υNH_2		

[46] and Hossain et al. [47], the mode υCOO^- was assigned to the bands at 1410 and 1560 cm^{-1}, $\delta N\text{-}H$ at 1450 cm^{-1}, and υCH at 2930 and 2970 cm^{-1}.

A comparison of the Raman spectra of ML, graphene and the 1 wt% dispersion can be seen in Fig. 2b. The Raman spectrum of the dispersion is a combination of those of neat ML and graphene. The peaks observed by the presence of the ionic liquid remain similar to those of neat ML. However, there are interesting differences in graphene. Graphene presents three peaks at 1350, 1580 and 2690 cm^{-1} [48], which correspond to D, G and 2D bands, respectively. When graphene was dispersed in ML, some considerable changes were found. The I_D/IG ratio is 1.08 for neat graphene and 1.42 for dispersion. The intensity of the D band is related to the presence of structural defects in graphene, which is a representation of the formation of different types of bonding. Such an increase implies a weakening in the graphene structure, i.e., a higher interaction with the ionic liquid enhanced by intercalation processes [49]. Thus, the stability of the dispersion can be explained by the interaction of ML with the surface of graphene.

5. Rheology

The addition of graphene to ML showed a remarkable effect on viscosity. In this study, we used concentration values of 0.1, 0.5 and 1 wt% to explore the concentration effect on the viscoelastic behaviour of this ionic liquid. Steady-state tests under increasing shear stress were conducted at a constant temperature of 25 °C.

ML presents a slight shear thinning effect [50], and this behaviour continues when a low concentration of graphene of 0.1 wt % was added. As can be seen in Fig. 3a, the viscosity values of pure ML and the dispersion with the lowest concentration of graphene nearly overlap, but some differences were found when a deeper analysis of the data was made, as we discuss below. However, when larger amounts of graphene were added a different scenario emerges. The resulting dispersions (0.5 and 1 wt%) presented higher values of viscosity than ML and a strong shear-thinning effect. Larger quantities of graphene motivate higher values of viscosity. This observation can be ascribed to two possible effects: the addition of the nanophase leads to more ordered structures [51], and/or particle–particle interactions provoke large aggregates [52], although both situations can be simultaneous and not competing. When high values of shear rate were applied, a drop in the viscosity was seen and a shear-thinning effect was appreciated. Since the final viscosity of these dispersions did not reach the ML constant values, it is more likely that graphene-graphene interactions were not completely suppressed.

Fig. 3b depicts the values of applied stress with increasing shear rate. ML and the dispersion with 0.1 wt% of graphene are Newtonian fluids, showing a linear dependence. Meanwhile, a non-Newtonian behaviour is seen for the dispersions with a higher concentration of graphene. These data were fitted to the Ostwald-de-Waele model (Equation (1)) and the results are collected in Table 2. This effect is of great importance for the performance of the nanofluids in tribological or heat and mass transfer applications. ML and the 0.1 wt% dispersion presented a value of n close to 1, as was expected for Newtonian fluids. It is interesting to point out that this dispersion with a very low quantity of graphene presents lightly lower values of viscosity than neat ML. Although the difference is not very high, the effect is more obvious in the values of A shown in Table 2. ML is composed of two small ions and its structure might be similar to ionic clusters [53], with hydrogen bonding as the dominant interactions over electrostatic forces. A weakening of hydrogen bonds in the structure of the ionic liquid due to the presence of small quantities of graphene could be the explanation for this viscosity decrease. On the other hand, the dispersion with 0.5 wt% G showed a value of n equal to 0.762, typical in pseudoplastic fluids. In the case of the dispersion with 1 wt%, the quality of the fitting was poorer (R^2 = 0.9185). The existence of a yield stress value can be recognized in Fig. 3b, and the data were satisfactorily fitted to a Herschel-Bulkley model (Equation (2)). Therefore, we can model this dispersion with a value of yield stress of 19 Pa and a deviation from the Newtonian behaviour with an n parameter of 0.672.

$$\tau = A \cdot \dot{\gamma}^n \tag{1}$$

$$\tau = \tau_o + A \cdot \dot{\gamma}^n \tag{2}$$

The presence of yield stress in nanofluids based on ionic liquids is commonly ascribed to an increase in the particle–particle interaction with increasing concentrations [52] and the percolation concentration is reached at some point between 0.5 and 1 wt% of graphene [54]. This effect is suppressed at high shear rates due to the disruption of the three-dimensional framework of the particles. Thus, the viscoelasticity of the dispersion is governed by the rheological behaviour of the neat ionic liquid.

We evaluated the viscoelastic behaviour by means of a creep-recovery test at room temperature. Several tests were attempted with all the samples, but only the nanofluid with 1 wt% showed a recovering behaviour. This is due to the low viscosity values of the rest of the samples and the lack of a three-dimensional structure with elastic recovery. In this test, constant shear stress of 1 Pa was applied for 5 min. The recovery of the samples was also recorded during 5 min. The creep and recovery curve can be seen in Fig. 4a, using the normalized strain versus time. We have calculated the elastic deformation, Yo, and the reversible deformation, Y_R, as it is explained by Amann et al. [54]. In this case, the elastic deformation is 0.81, i.e., there is a recovery of 81 % when the stress is suppressed, and the reversible deformation is 0.47. Therefore, this nanofluid presents a high reversible deformation when low shear stress is applied.

In order to set a mechanical model for this nanofluid, both the elastic and viscous moduli must be taken into account. In this case, it was found that the data of both creep and recovery were successfully fitted to a unique complex Burgers model depicted in Scheme 2 [55]. The Maxwell element is composed of one ideal spring (EM) followed by one hydraulic damper (η_M), describing the instantaneous deformation in soft solids. On the other hand, the Kelvin-Voigt element is represented by the same elements but arranged in parallel (E_{KV} and η_{KV}) and is related to the creep of the sample. In scheme 2, it is seen how the Maxwell and Kelvin-Voigt elements are placed, with a damper followed by two Kelvin-Voigt elements. The model is mathematically described by Equations (3) (creep) and (4) (recovery) and the fitting line can be observed in Fig. 4b. This model was able to describe both creep

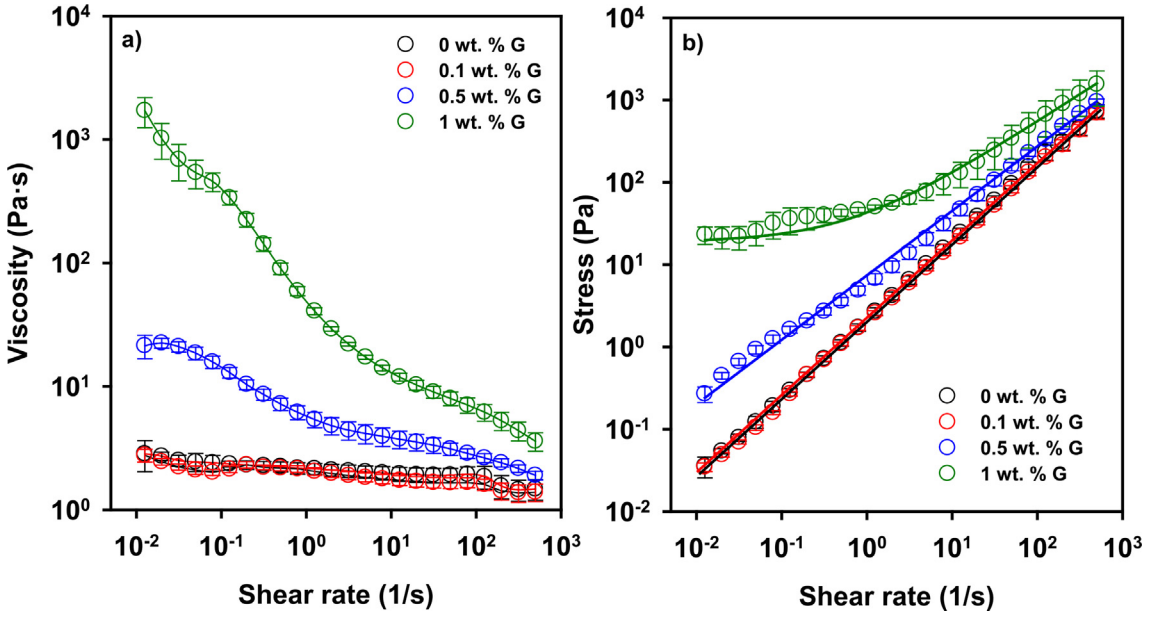

Fig. 3. a) Shear rate dependence on viscosity and b) applied stress of ML with 0, 0.1, 0.5 and 1 wt% of graphene.

Table 2
Ostwald-de Waele parameters values calculated for the samples with 0, 0.1 and 0.5 wt% graphene, and Herschel-Bulkley parameters fitted for the sample with 1 wt% of graphene.

Graphene wt.%	Ostwald-de Waele			
	A (Pa·s)	n		R^2
0	2.18 ± 0.02	0.951 ± 0.002		0.9997
0.1	1.99 ± 0.02	0.948 ± 0.003		0.9997
0.5	7.3 ± 0.2	0.762 ± 0.008		0.9954
Graphene wt.%	**Herschel-Bulkley**			
	τ_o (Pa)	A (Pa·s)	n	R^2
1	19 ± 3	24 ± 1	0.672 ± 0.009	0.9984

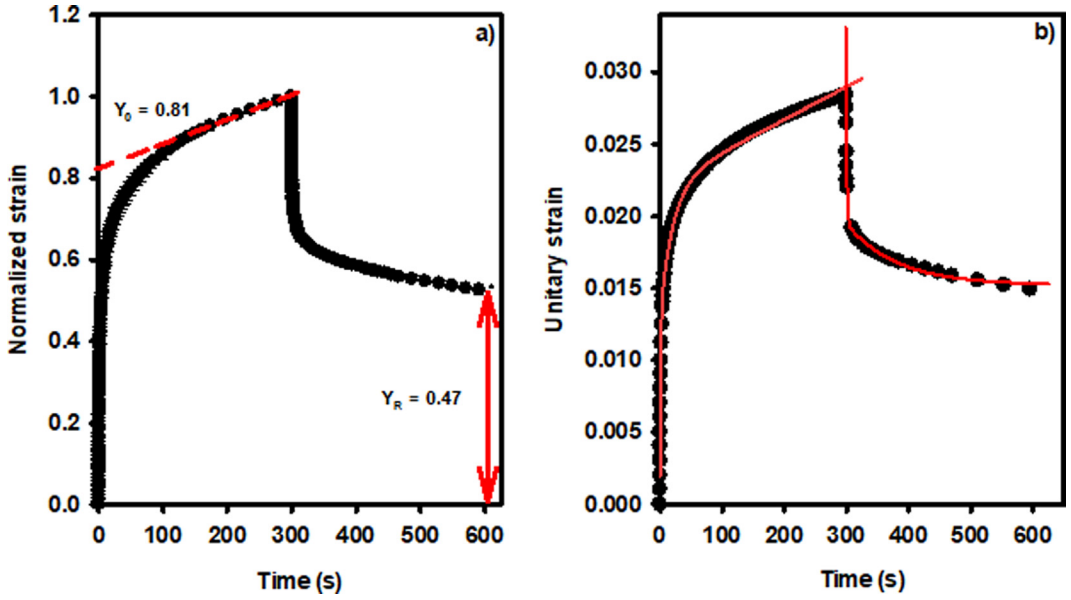

Fig. 4. a) Creep-recovery test of the nanofluid with 1 wt% G and b) fitting to the complex Burgers model.

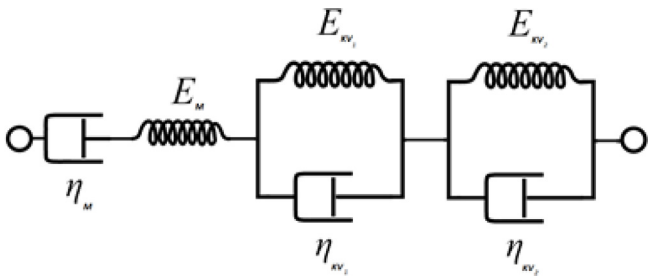

Scheme 2. Maxwell and Kelvin-Voigt elements distribution in the complex Burgers model.

Table 3
Fitting parameters of the complex Burgers model for the creep and recovery of the ML dispersion with 1 wt% of graphene.

Element	Property	Creep	Recovery
Maxwell	E_M (Pa)	510 ± 30	–
	η_M (Pa·s)	44000 ± 1000	19700 ± 100
	μ_o (s)	44000 ± 1000	19700 ± 100
First Kelvin-Voigt	E_{KV1} (Pa)	110 ± 2	230 ± 5
	η_{KV1} (Pa·s)	2300 ± 100	21000 ± 1000
	λ_1 (s)	21	91
Second Kelvin-Voigt	E_{KV2} (Pa)	90 ± 2	146 ± 3
	η_{KV2} (Pa·s)	115 ± 8	210 ± 10
	λ_2 (s)	1.3	1.4

and recovery behaviour of the dispersion with 1 wt% of graphene. The constants of these fittings are collected in Table 3, and the coefficient of determination (R^2) were 0.9971 for the creep and 0.9842 for the recovery.

these two domains are sufficiently different, the response to a physical perturbation could be different as well [56].

The effect of temperature on the viscosity was evaluated in the range of 20 to 110 °C with a linear increase of 3 °C/min at a constant shear rate of 50 s^{-1}. All samples showed a similar trend, and a decrease in viscosity with increasing temperature is observed in Fig. 5a. The drop in viscosity at room temperature, when 0.1 wt% of graphene is added, seen in the steady state viscosity is now more obvious when the temperature effect is taken into account, as it is observed in Fig. 5a. When the temperature is raised, the weakening of the interactions of the ionic liquid are suppressed and the reinforcing effect of the addition of graphene is dissipated. However, this dissipation was less pronounced when 1 wt% of graphene was added, and a pseudo-asymptotic behaviour was found.The data were satisfactorily fitted to different Vogel-Fulcher-Tammann (VFT) model [57–59] (Equation (5)).

$$\eta = A_\eta e^{\frac{k_\eta}{T-T_o}} \tag{5}$$

Model VFT was conceived for glass materials, but it has been previously used to describe the thermal behaviour of different ionic liquids and dispersions [43,60]. In this model, the parameter A_η represents the viscosity when the temperature tends to infinite; k_η is a measure of the thermal sensitivity of the fluid and T_o is the theoretical temperature at which the sample begins to flow. We have also calculated the strength index D as k_η / T_o. These data are summarized in Table 4 with similar values compared to other PILs found in the literature [61,62]. As expected, A_η and T_o increase with the addition of graphene, and k_η decreased. Thus, this nanophase not only increases the viscosity but also the thermal stability of the nanofluid. Large concentrations of graphene in ML imply a lower influence of the temperature on the flow behaviour. On the other hand, D decreased with the addition of graphene. According to the literature [63,64], ML presents a high value of the strength index compared to other ionic liquids. Fluids with large values of D are soft materials with directional intermolecular bonding [50,65]. Therefore, the decrease of D when graphene was added could be explained by stronger interactions on the nanofluid with non-directional bonds, i.e., the dispersion presents a stronger three-dimensional structure.

$$\varepsilon(t,\sigma_o) = \frac{\sigma_o}{E_M} + \frac{\sigma_o}{\eta_M}\cdot t + \frac{\sigma_o}{E_{KV1}}\cdot\left(1 - e^{\frac{-E_{KV1}}{\eta_{KV1}}\cdot t}\right) + \frac{\sigma_o}{E_{KV2}}\cdot\left(1 - e^{\frac{-E_{KV2}}{\eta_{KV2}}\cdot t}\right) \tag{3}$$

$$\varepsilon(t,\sigma_o) = \frac{\sigma_o}{\eta_M}\cdot(t - t_{CR}) + \frac{\sigma_o}{E_{KV1}}\cdot\left(1 - e^{\frac{-E_{KV1}}{\eta_{KV1}}\cdot t_{CR}}\right)\cdot e^{\frac{-E_{KV1}}{\eta_{KV1}}\cdot(t-t_{CR})} + \\ + \frac{\sigma_o}{E_{KV2}}\cdot\left(1 - e^{\frac{-E_{KV2}}{\eta_{KV2}}\cdot t_{CR}}\right)\cdot e^{\frac{-E_{KV2}}{\eta_{KV2}}\cdot(t-t_{CR})} \tag{4}$$

Additionally, we can define the relaxation time for each element. For the Maxwell element, the relaxation time (μ_o) is the ratio η_M/σ_o and in the case of the Kelvin-Voigt elements, the retardation time (λ_i) is defined as the ratio η_{KVi}/ E_{KVi}.

The complexity of the model reflects the intricate rheological performance of this dispersion. The lack of uniformity in the fluid might be the reason for the anomalous viscosity behaviour. The presence of two Kelvin-Voigt elements could be related to two different retardation processes and different domains with distinct molecular arrangements. This behaviour could be related to the presence of domains with completely dispersed graphene sheets with faster relaxation (λ_2), and domains containing agglomerates of graphene in ML with larger values of retardation time (λ_1). If

Further information was obtained when the viscosity data were fitted to the temperature Power Law model (Equation (6)).

$$\eta = \eta_o\left(\frac{T - T_x}{T_x}\right)^{-\gamma} \tag{6}$$

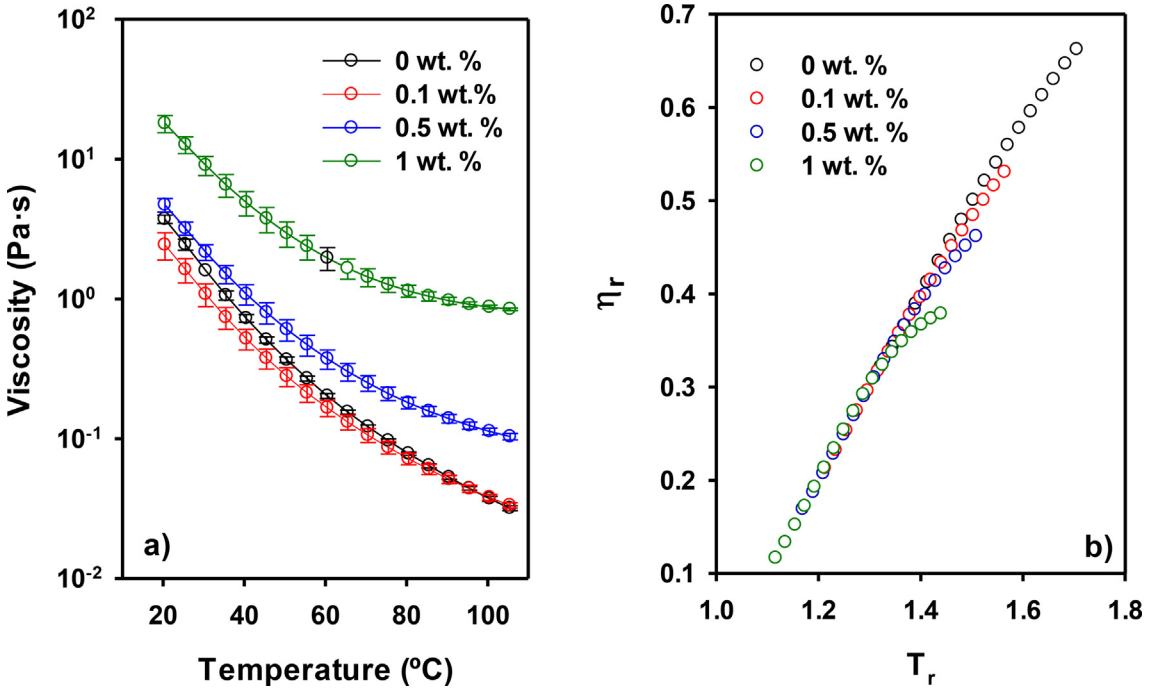

Fig. 5. a) Temperature dependence of viscosity at 50 s^{-1} and b) master curves for ML and ML-G dispersions.

Table 4
VFT and Power Law fitting parameters for the ML nanofluids with 0, 0.1, 0.5 and 1 wt% of graphene. The coefficients of determination are available in Table S1 in the Supporting Information.

wt. % of graphene	Vogel-Fulcher-Tammann				Power Law		
	$A_\eta \cdot 10^4$ (Pa s)	k_η (K)	T_o (K)	D	$\eta_o \cdot 10^4$ (Pa s)	T_x (K)	γ
0	0.020 ± 0.007	2300 ± 100	136 ± 4	16.9 ± 0.9	21 ± 2	222 ± 2	6.6 ± 0.2
0.1	0.53 ± 0.08	1280 ± 40	174 ± 2	7.4 ± 0.2	17.0 ± 0.2	242 ± 1	4.70 ± 0.09
0.5	6.0 ± 0.7	920 ± 30	191 ± 2	4.8 ± 0.2	55 ± 1	251 ± 1	3.84 ± 0.08
1	290 ± 30	510 ± 20	215 ± 2	2.4 ± 0.1	680 ± 30	263 ± 1	2.62 ± 0.07

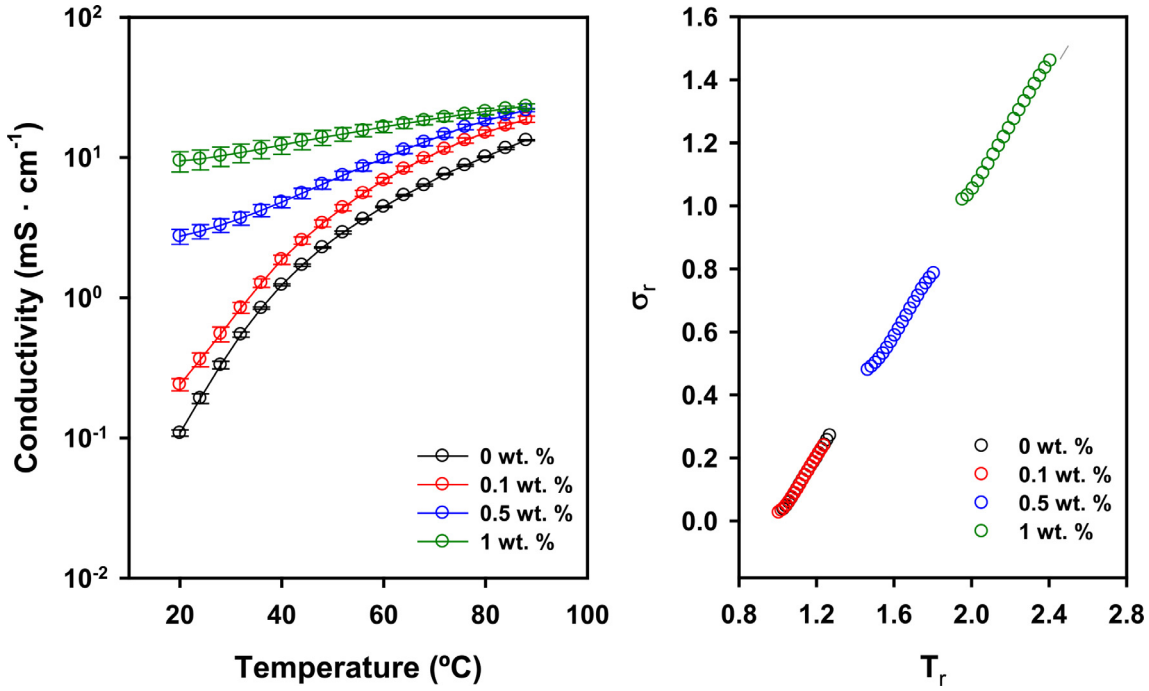

Fig. 6. a) Temperature dependence of electrical conductivity and b) master curves for ML and ML-G dispersions.

Table 5
VFT and Power Law fitting parameters using electrical conductivity data for the ML nanofluids with 0, 0.1, 0.5 and 1 wt% graphene. The coefficients of determination are available in Table S1 in the Supporting Information.

wt. % of graphene	Vogel-Fulcher-Tammann			Power Law			
	$A_\sigma \cdot 10^3$ (mS/cm)	k_σ (K)	T_o (K)	D	$\sigma_o \cdot 10^3$ (mS/cm)	T_x (K)	γ
0	45 ± 4	1820 ± 20	136 ± 4	13.4 ± 0.5	0.311 ± 0.002	284.3 ± 0.3	2.41 ± 0.01
0.1	8.9 ± 0.7	1150 ± 10	174 ± 2	6.6 ± 0.1	0.320 ± 0.08	291.2 ± 0.7	1.98 ± 0.03
0.5	1.0 ± 0.7	651 ± 7	191 ± 2	3.41 ± 0.07	0.06 ± 0.03	200 ± 10	4.2 ± 0.4
1	0.074 ± 0.002	175 ± 3	215 ± 2	0.81 ± 0.02	0.009 ± 0.004	150 ± 10	2.5 ± 0.2

In this model, η_o represents the asymptote value, T_x is a threshold temperature at which the sample becomes fragile and γ is the parameter that modulates the effect of the temperature on the viscosity. In agreement with the VFT model, the addition of graphene provokes an increase in viscosity and a decrease in the thermal sensitivity of the nanofluid. This model also allowed us to construct a master curve using the relative viscosity, η_r, and relative temperature, T_r, described by Equations (7) and (8).

$$\eta_r = \left(\frac{\eta}{\eta_o}\right)^{-1/\gamma} \tag{7}$$

$$T_r = \frac{T}{T_x} \tag{8}$$

The master curves are shown in Fig. 5b. According to [50], this kind of representation has been satisfactorily used in ionic liquids. However, the effect of the addition of nanomaterials has not been tested yet, to the best of our knowledge. In the case of pure ML, we found a good agreement with the model, as expected. It is clearly seen that the addition of graphene causes a deviation in the model, which is in agreement with the viscosity results previously shown. Since graphene reduces the effect of temperature on the viscosity of the nanofluid, this deviation of the master curves occurred when the temperature was raised. This effect was more evident when larger concentrations of graphene were considered.

6. Electrical conductivity

Fig. 6a shows the evolution of the electrical conductivity values for the pure ionic liquid and the dispersions with different amounts of graphene. As expected, the conductivity values increase with temperature and with the amount of graphene added to the dispersion. At 20 °C, the conductivity of the dispersion with only 0.1 wt% is 0.1 mS/cm, very similar to that of the pure ionic liquid (0.24 mS/cm). However, the dispersion with 0.5 wt% has a conductivity value of 2.7 mS/cm and the 1 wt% dispersion reaches 9.4 mS/cm, which is a severe increase for the small amount of graphene added. The distance between the graphene sheets decreases in the more concentrated dispersions and they form an efficient conductive pathway in the IL matrix, which contributes to increasing the electrical conductivity.

As in the case of the viscosity data, the electrical conductivity data have been fitted using the VFT model shown in Equation (9).

$$\sigma = A_\sigma \cdot e^{\frac{-k_\sigma}{T-T_o}} \tag{9}$$

From the fitting of the experimental data to this semi-phenomenological equation, we will extract the parameter A_σ which represents the conductivity when the temperature tends to infinite and k_σ is a measure of the thermal sensitivity of the fluid, i.e., the activation energy for conduction. T_o has an analogous meaning as in the viscosity data [66,67] resembled the glass transition temperature [68]. In this study, the same values have been used as those obtained in the viscosity section [69].

We also calculated the strength index D as k_σ / T_o. In Table 5, it can be seen that the values of A_σ, k_σ and D decreased with the addition of graphene. As in the case of viscosity, large concentrations of graphene in ML imply also a lower influence of the temperature on the conductivity. The conductivity data could also be fitted using the Power Law model analogously to the viscosity data, as can be observed in Table 5. To the best of our knowledge, this model has never been used to describe the behaviour of the conductivity in nanofluids. In this case σ_o represents the conductivity asymptote value and T_x and γ maintain the same meaning as in the viscosity section. T_x and σ_o values decrease with increasing graphene content. Fig. 6b shows the master curves that could be obtained, presenting a linear trend. σ_r was calculated according to Equation (10). The data for the pure ionic liquid and the dispersion with the lowest amount of graphene overlap due to the relatively similar conductivity values. In the case of the addition of 0.5 and 1 wt% graphene, the conductivity master curves do not overlap. This is due to the large difference in their conductivity values, as seen in Fig. 6a.

$$\sigma_r = \left(\frac{\sigma}{\sigma_o}\right)^{-\gamma} \tag{10}$$

7. Electrochemical characterisation

Electrochemical characterisation of the ionic liquid and dispersions has also been carried out by cyclic voltammetry as shown in Fig. 7. As can be observed, the behaviour of the neat ionic liquid and the dispersions with 0.1 and 0.5 % graphene are very similar. When the potentials are shifted towards more positive values, irreversible oxidation is observed at 2 V, probably due to the irreversible oxidation of water content of the ionic liquid. The forward and reverse curves nearly overlap. The oxidation of the ionic liquid seems to start circa 4 V. Conversely, the behaviour of the dispersion with 1 % graphene is very different because the percolated state is reached in agreement with the rheological data. In this case, an intense oxidation is observed at lower potentials, around 1 V. This would indicate that for this dispersion there is sig-

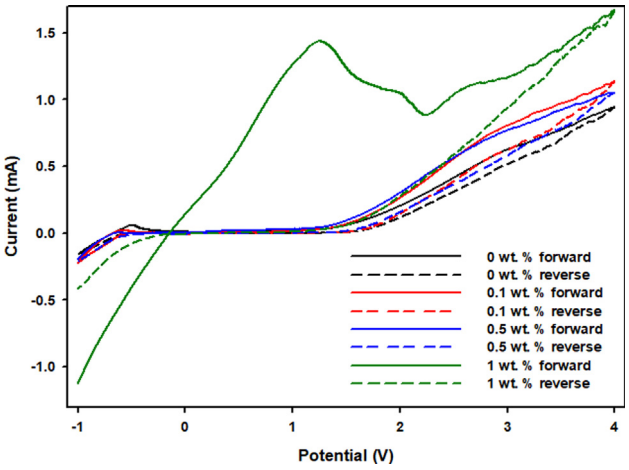

Fig. 7. Cyclic voltammograms of ML nanofluids with 0, 0.1, 0.5 and 1 wt% of graphene at 10 mVs^{-1}.

nificant oxidation of the graphene present in the dispersion, which is not observed at lower concentrations.

8. Conclusions

2-hydroxyethylammonium lactate ionic liquid was utilised to disperse graphene, using concentrations of 0.1, 0.5 and 1 wt%. The dispersion of graphene in ML was confirmed by FT-IR and Raman spectroscopies, and the dispersions were stable for, at least, 2 months of observation.

The steady-state viscosity measurements showed that ML is a Newtonian fluid and the addition of 0.1 wt% of graphene does not significantly change this behaviour. However, there is a drop in the viscosity values ascribed to the suppression of hydrogen bonding of the ionic liquid. When the concentration is increased, a non-Newtonian behaviour is observed. The dispersion with 0.5 wt% of graphene was fitted to a typical Ostwald model, but when 1 wt% of graphene was added, a yield stress was observed due to the increase of the particle–particle interactions. Creep-recovery tests at room temperature were conducted for the nanofluid with 1 wt% of graphene. The data were adequately fitted to a complex Burgers model and a reversible deformation of 47 % was found, showing a strong viscoelastic response in agreement with the previous rheological results. The complexity of the rheological performance of this dispersion could be ascribed to different structural arrangements in the nanofluid, such as domains with highly dispersed nanomaterial with few layers of graphene showing a faster relaxation, and regions with larger nanoparticles with a slower viscoelastic response.

The temperature dependence of the viscosity and conductivity were also evaluated and VFT model was used to describe the thermal response. The temperature dependence on the fitting parameters is suppressed by the increasing addition of graphene. According to the rheological analysis, ML behaves as a soft fluid, and graphene acts as a severe strengthening additive of the fluid, indicating that the percolation concentration is reached in the range of 0.5 to 1 wt%.

A Power Law was also utilised to describe the thermal behaviour and construct master curves. ML was perfectly depicted by this model, but when the concentration of graphene was raised, stronger deviations were found. This finding is in agreement with the lower thermal effect observed with the VFT model.

Electrochemical characterisation of the dispersions indicates that ML and the dispersions with 0.1 and 0.5 wt% of graphene show a similar trend with an irreversible oxidation at 2 V probably due to small quantities of water. On the other hand, the dispersion with higher graphene content (1 wt%), exhibits an intense oxidation around 1 V. To the best of our knowledge, this behaviour has not been observed before and could be related to the exceeding of the percolation concentration, allowing a higher amount of graphene to be oxidised.

In summary, graphene is appropriately dispersed in ML and this ionic liquid is a suitable and environmentally friendly option to produce stable graphene-based nanofluids. Increasing the concentration of graphene provokes interesting viscoelastic and electrochemical behaviours and these nanofluids show potential applications in different fields such as incorporation into polymeric matrices, advanced lubricants or energy storage.

Funding resources

The authors acknowledge the financial support of Ministerio de Economía y Competitividad and Agencia Estatal de Investigación (MINECO and AEI, Spain), EU-FEDER (MAT2017-85130-P, and PID2021-122169NB) and the Fundación Seneca, Agencia de Ciencia y Tecnología de la Región de Murcia ('Ayuda a las Unidades y Grupos de Excelencia Científica de la Región de Murcia'; Grant # 19877/GERM/15). P.M. M.-R. is grateful to Fundación Séneca for FPI research grant (21574/FPI/21).

CRediT authorship contribution statement

Pablo Manuel Martínez-Rubio: Methodology, Investigation. **María Dolores Avilés:** Methodology. **Joaquín Arias-Pardilla:** Methodology, Investigation, Writing – original draft. **Francisco José Carrión-Vilches:** . **José Sanes:** . **María Dolores Bermúdez:** Conceptualization, Validation, Formal analysis, Resources, Writing – original draft. **Ramón Pamies:** Methodology, Conceptualization, Validation, Formal analysis, Investigation, Resources, Writing – original draft.

Data availability

Data will be made available on request.

Declaration of Competing Interest

The authors declare that they have no known competing financial interests or personal relationships that could have appeared to influence the work reported in this paper.

Appendix A. Supplementary material

Supplementary data to this article can be found online at https://doi.org/10.1016/j.molliq.2022.120446.

References

[1] K.S. Novoselov, A.K. Geim, S.V. Morozov, D. Jiang, Y. Zhang, S.V. Dubonos, I.V. Grigorieva, A.A. Firsov, Electric field effect in atomically thin carbon films, Science 306 (5696) (2004) 666–669.
[2] R.N. Queiroz, P. Prediger, M.G.A. Vieira, Adsorption of polycyclic aromatic hydrocarbons from wastewater using graphene-based nanomaterials synthesized by conventional chemistry and green synthesis: a critical review, J. Hazard. Mater. 422 (2022) 126904.
[3] H.-W. Lu, A.A. Kane, J. Parkinson, Y. Gao, R. Hajian, M. Heltzen, B. Goldsmith, K. Aran, The promise of graphene-based transistors for democratizing multiomics studies, Biosens. Bioelectron. 195 (2022) 113605.
[4] L.Y. Wong, S.Y. Lau, S. Pan, M.K. Lam, 3D graphene-based adsorbents: Synthesis, proportional analysis and potential applications in oil elimination, Chemosphere 287 (2022) 132129.
[5] J. Sanes, C. Sanchez, R. Pamies, M. D. Aviles, M.D. Bermudez, Extrusion of Polymer nanocomposites with graphene and graphene derivative nanofillers: an overview of recent developments, Materials 13(3) (2020), doi: 10.3390/ma13030549.
[6] G. Yang, L.H. Li, W.B. Lee, M.C. Ng, Structure of graphene and its disorders: a review, Sci. Technol. Adv. Mater. 19 (1) (2018) 613–648, https://doi.org/10.1080/14686996.2018.1494493.
[7] A.G. Olabi, M.A. Abdelkareem, T. Wilberforce, E.T. Sayed, Application of graphene in energy storage device – a review, Renew. Sustain. Energy Rev. 135 (2021) 110026.
[8] M. G. Burdanova, M. V Kharlamova, C. Kramberger, M.P. Nikitin, Applications of pristine and functionalized carbon nanotubes, graphene, and graphene nanoribbons in biomedicine, Nanomaterials 11(11) (2021), doi: 10.3390/nano11113020.
[9] M. Kaur, M.K. Ubhi, J.K. Grewal, V.K. Sharma, Boron- and phosphorous-doped graphene nanosheets and quantum dots as sensors and catalysts in environmental applications: a review, Environ. Chem. Lett. 19 (6) (2021) 4375–4392, https://doi.org/10.1007/s10311-021-01281-0.
[10] J. Li, H.P. Zheng, L. Liu, F.D. Meng, Y. Cui, F.H. Wang, Modification of graphene and graphene oxide and their applications in anticorrosive coatings, J. Coat. Technol. Res. 18 (2) (2021) 311–331, https://doi.org/10.1007/s11998-020-00435-z.
[11] M. Kharazi, J. Saien, S. Asadabadi, Review on amphiphilic ionic liquids as new surfactants: from fundamentals to applications, Top Curr Chem (Z) 380 (1) (2022).
[12] E. Amini, C. Valls, M.B. Roncero, Ionic liquid-assisted bioconversion of lignocellulosic biomass for the development of value-added products, J. Clean Prod. 326 (2021) 129275.
[13] Y.L. Kobzar, K. Fatyeyeva, Ionic liquids as green and sustainable steel corrosion inhibitors: recent developments, Chem. Eng. J. 425 (2021) 131480.
[14] T.L. Greaves, C.J. Drummond, Protic ionic liquids: evolving structure-property relationships and expanding applications, Chem. Rev. 115 (20) (2015) 11379–11448, https://doi.org/10.1021/acs.chemrev.5b00158.

[15] V.H. Alvarez et al., Bronsted Ionic Liquids for Sustainable Processes: Synthesis and Physical Properties, J Chem Eng Data, vol. 55, no. Iberian Meeting on Ionic Liquids (IMIL), pp. 625–632, 2010, doi: 10.1021/je900550v.
[16] A. Kumar, D. Pratap Singh, G. Singh, Recent progress and future perspectives on carbon-nanomaterial-dispersed liquid crystal composites, J. Phys. D Appl. Phys. 55 (8) (2022) 083002.
[17] M. Faizan, R. Ahmed, H.M. Ali, A critical review on thermophysical and electrochemical properties of Ionanofluids (nanoparticles dispersed in ionic liquids) and their applications, J. Taiwan Inst. Chem. Eng. 124 (2021) 391–423, https://doi.org/10.1016/j.jtice.2021.02.004.
[18] Y.H. Zhao, Z.H. Hu, Graphene in ionic liquids: collective van der waals interaction and hindrance of self-assembly pathway, J. Phys. Chem. B 117 (36) (2013) 10540–10547, https://doi.org/10.1021/jp405660d.
[19] V.S. Anithaa, R. Shankar, S. Vijayakumar, Structural and electronic properties of graphene and its derivatives physisorbed by ionic liquids, Diam. Relat. Mater. 109 (2020) 108005.
[20] C. Hermida-Merino et al., Graphene IoNanofluids, thermal and structural characterization, Nanomaterials 9(11) (2019), doi: 10.3390/nano9111549.
[21] C.N. de Castro, A.P. C. Ribeiro, S. I.c., J.M. P. Franca, M. J.v., F. V., S. M.s, P. Goodrich, C. Hardacre, Ionic Liquids - New Aspects for the Future, InTech, 2013.
[22] J. Kim, H. Park, Enhanced mass transfer in nanofluid electrolytes for aqueous flow batteries: The mechanism of nanoparticles as catalysts for redox reactions, J Energy Storage 38 (2021) 102529.
[23] X. Lu, Z. Lu, R. Zhang, L. Zhao, H. Xie, Distribution of pigments in the aqueous two-phase system formed with piperazinium-based ionic liquid and anionic surfactant, J. Mol. Liq. 330 (2021) 115677.
[24] E. Aali, M. Gholizadeh, N. Noroozi-Shad, 1-Disulfo-[2,2-bipyridine]-1,1-diium chloride ionic liquid as an efficient catalyst for the green synthesis of 5-substituted 1 H-tetrazoles, J. Mol. Struct. 1247 (2022) 131289.
[25] Y.Q. Rao, Nanofluids: stability, phase diagram, rheology and applications, Particuology 8 (6) (2010) 549–555, https://doi.org/10.1016/j.partic.2010.08.004.
[26] R. Pamies, M.D. Avilés, J. Arias-Pardilla, T. Espinosa, F.J. Carrión, J. Sanes, M.D. Bermúdez, Antiwear performance of ionic liquid+graphene dispersions with anomalous viscosity-temperature behavior, Tribol. Int. 122 (2018) 200–209.
[27] V. Singh, K.D. Amirchand, R.L. Gardas, Ionic liquid-nanoparticle based hybrid systems for energy conversion and energy storage applications, J. Taiwan Inst. Chem. Eng. 133 (2022) 104237.
[28] A.v Agafonov, E.P. Grishina, N.O. Kudryakova, L.M. Ramenskaya, A.S. Kraev, V.D. Shibaeva, Ionogels: Squeeze flow rheology and ionic conductivity of quasi-solidified nanostructured hybrid materials containing ionic liquids immobilized on halloysite, Arab. J. Chem. 15(1) (2022), doi: 10.1016/j.arabjc.2021.1034701878-5352.
[29] S. Aberoumand, P. Woodfield, G.e. Shi, T. Kien Nguyen, H.-Q. Nguyen, Q. Li, B. Shabani, D. Viet Dao, Thermo-electro-rheological behaviour of vanadium electrolyte-based electrochemical graphene oxide nanofluid designed for redox flow battery, J. Mol. Liq. 338 (2021) 116860.
[30] B. Jóźwiak, S. Boncel, Rheology of ionanofluids – a review, J. Mol. Liq. 302 (2020) 112568.
[31] L.H. Kumar, S.N. Kazi, H.H. Masjuki, M.N.M. Zubir, A review of recent advances in green nanofluids and their application in thermal systems, Chem. Eng. J. 429 (2022), https://doi.org/10.1016/j.cej.2021.132321 132321.
[32] P. Estellé, G. Żyła, Advances in rheological behavior of nanofluids and ionanofluids – an editorial note, J. Mol. Liq. 362 (2022) 119669.
[33] M.-D. Avilés, R. Pamies, J. Sanes, M.-D. Bermúdez, Graphene-ionic liquid thin film nanolubricant, Nanomaterials 10(3) (2020), doi: 10.3390/nano10030535.
[34] E. Fabre, S.M.S. Murshed, A comprehensive review of thermophysical properties and prospects of ionanocolloids in thermal energy applications, Renew. Sustain. Energy Rev. 151 (2021) 111593.
[35] S. Pavlovica, A. Zicmanis, E. Gzibovska, M. Klavins, P. Mekss, "(2-Hydroxyethyl) ammonium lactates—highly biodegradable and essentially non-toxic ionic liquids, Green Sustain. Chem. 01 (03) (2011) 103–110.
[36] S. Barros, R.S. Andrade, M. Iglesias, Effect of temperature on thermodynamic properties of protic ionic liquids: 2-hydroxy ethylammonium lactate (2-HEAL), Int. J. Thermodyn. 21 (2) (2018) 70–80, https://doi.org/10.5541/ijot.303607.
[37] R.S. Andrade, D. Torres, F.R. Ribeiro, B.G. Chiari-Andreo, J.A. Oshiro, M. Iglesias, Sustainable cotton dyeing in nonaqueous medium applying protic ionic liquids, ACS Sustain. Chem. Eng. 5 (10) (2017) 8756–8765, https://doi.org/10.1021/acssuschemeng.7b01555.
[38] N. Saurín, M.D. Avilés, T. Espinosa, J. Sanes, F.J. Carrión, M.D. Bermúdez, P. Iglesias, Carbon nanophases in ordered nanofluid lubricants, Wear 376-377 (2017) 747–755.
[39] J. Sanes, M.D. Aviles, N. Saurin, T. Espinosa, F.J. Carrion, M.D. Bermudez, Synergy between graphene and ionic liquid lubricant additives, Tribol. Int. 116 (2017) 371–382, https://doi.org/10.1016/j.triboint.2017.07.030.
[40] M.R. Esfahani, E.M. Languri, M.R. Nunna, Effect of particle size and viscosity on thermal conductivity enhancement of graphene oxide nanofluid, Int. Commun. Heat Mass Transfer 76 (2016) 308–315, https://doi.org/10.1016/j.icheatmasstransfer.2016.06.006.
[41] S. Hamze, D. Cabaleiro, P. Estellé, Graphene-based nanofluids: a comprehensive review about rheological behavior and dynamic viscosity, J. Mol. Liq. 325 (2021) 115207.
[42] R. Pamies, C. Espejo, F.J. Carrión, A. Morina, A. Neville, M.D. Bermúdez, Rheological behavior of multiwalled carbon nanotube-imidazolium tosylate ionic liquid dispersions, J. Rheol. 61 (2) (2017) 279–289.
[43] R. Pamies, M.D. Avilés, J. Arias-Pardilla, F.J. Carrión, J. Sanes, M.D. Bermúdez, Rheological study of new dispersions of carbon nanotubes in the ionic liquid 1-ethyl-3-methylimidazolium dicyanamide, J. Mol. Liq. 278 (2019) 368–375.
[44] G. Cassanas, M. Morlisi, E. Fabregue, L. Bardet, Vibartional-spectra of lactic-acid and lactates, J. Raman Spectrosc. 22 (7) (1991) 409–413, https://doi.org/10.1002/jrs.1250220709.
[45] M.K. Wong, M.A. Bustam, A.M. Shariff, Chemical speciation of CO2 absorption in aqueous monoethanolamine investigated by in situ Raman spectroscopy, Int. J. Greenhouse Gas Control 39 (2015) 139–147, https://doi.org/10.1016/j.ijggc.2015.05.016.
[46] D. Simijonovic, Z.D. Petrovic, V.P. Petrovic, Some physico-chemical properties of ethanolamine ionic liquids: behavior in different solvents, J. Mol. Liq. 179 (2013) 98–103, https://doi.org/10.1016/j.molliq.2012.12.020.
[47] M. Ismail Hossain, M. El-Harbawi, Y.A. Noaman, M.A.B. Bustam, N.B.M. Alitheen, N.A. Affandi, G. Hefter, C.-Y. Yin, Synthesis and anti-microbial activity of hydroxylammonium ionic liquids, Chemosphere 84 (1) (2011) 101–104.
[48] Y.-P. Childres, I. Jauregui, L.-A. Park, W. Cao, H. Chen, Raman spectroscopy of graphene and related materials, in: New developments in photon and materials research, 2013, pp. 1–20.
[49] L.Y. Zhao, R.Y. Zhang, C.Y. Deng, Y.X. Peng, T. Jiang, Tunable infrared emissivity in multilayer graphene by ionic liquid intercalation, Nanomaterials 9(8) (2019), doi: 10.3390/nano9081096.
[50] D. Camargo, R.S. Andrade, G.A. Ferreira, H. Mazzer, L. Cardozo, M. Iglesias, Investigation of the rheological properties of protic ionic liquids, J. Phys. Org. Chem. 29(Latin American Conference) (2016) 604–612, doi: 10.1002/poc.3553.
[51] A. Shakeel, H. Mahmood, U. Farooq, Z. Ullah, S. Yasin, T. Iqbal, C. Chassagne, M. Moniruzzaman, Rheology of pure ionic liquids and their complex fluids: a review, ACS Sustain Chem Eng 7 (16) (2019) 13586–13626.
[52] E. Altin, J. Gradl, W. Peukert, First studies on the rheological behavior of suspensions in ionic liquids, Chem. Eng. Technol. 29 (11) (2006) 1347–1354, https://doi.org/10.1002/ceat.200600135.
[53] R. Ludwig, A simple geometrical explanation for the occurrence of specific large aggregated ions in some protic ionic liquids, J. Phys. Chem. B 113 (47) (2009) 15419–15422, https://doi.org/10.1021/jp907204x.
[54] T. Amann, C. Dold, A. Kailer, Rheological characterization of ionic liquids and ionic liquid crystals with promising tribological performance, Soft Matter 8 (38) (2012) 9840–9846, https://doi.org/10.1039/c2sm26030a.
[55] C. Hermida-Merino, M. Perez-Rodriguez, M.M. Pineiro, M.J. Pastoriza-Gallego, Evidence of viscoplastic behavior of exfoliated graphite nanofluids, Soft Matter 12 (8) (2016) 2264–2275, https://doi.org/10.1039/c5sm02932e.
[56] M. Cacciola, M. Osaci, Studies about the influence of self-organization of colloidal magnetic nanoparticles on the magnetic N, el relaxation time, Colloid J. 78 (4) (2016) 448–458, https://doi.org/10.1134/S1061933X16040037.
[57] H. Vogel, Das temperaturabhängigkeitsgesetz der viskosität von flüssigkeiten, Physikalische Zeitschrift 22 (1921) 645–646.
[58] G.S. Fulcher, Analysis of recent measurements of the viscosity of glasses, J. Am. Ceram. Soc. 8 (6) (1925) 339–355, https://doi.org/10.1111/j.1151-2916.1925.tb16731.x.
[59] G. Tammann, W. Hesse, Die Abhängigkeit der Viscosität von der Temperatur bie unterkühlten Flüssigkeiten, Z. Anorg. Allg. Chem. 156 (1) (1926) 245–257.
[60] O.O. Okoturo, T.J. VanderNoot, Temperature dependence of viscosity for room temperature ionic liquids, J. Electroanal. Chem. 568 (1–2) (2004) 167–181, https://doi.org/10.1016/j.jelechem.2003.12.050.
[61] J.P. Belieres, C.A. Angell, Protic ionic liquids: preparation, characterization, and proton free energy level representation, J. Phys. Chem. B 111 (18) (2007) 4926–4937, https://doi.org/10.1021/jp067589u.
[62] F.F. Augusto, M. Francisco, E. Stephen, H. Jason, V.D.W. Luuk, W. Geert-Jan, F.M. Bruno, Physicochemical characterization of two protic hydroxyethylammonium carboxylate ionic liquids in water and their mixture, J. Chem. Eng. Data 67 (6) (2022) 1309–1325.
[63] X.J. Wang, Y.L. Chi, T.C. Mu, A review on the transport properties of ionic liquids, J. Mol. Liq. 193 (2014) 262–266, https://doi.org/10.1016/j.molliq.2014.03.011.
[64] D. Rauber et al., Structure-property relation of trimethyl ammonium ionic liquids for battery applications, Appl. Sci. 11 (1)2 (2021), doi: 10.3390/app11125679.
[65] R. Bohmer, K.L. Ngai, C.A. Angell, D.J. Plazek, Non-expontential relaxations in strong and fragile glass formers, J. Chem. Phys. 99 (5) (1993) 4201–4209, https://doi.org/10.1063/1.466117.
[66] J. Vila, L.M. Varela, O. Cabeza, Cation and anion sizes influence in the temperature dependence of the electrical conductivity in nine imidazolium based ionic liquids, Electrochim. Acta 52 (26) (2007) 7413–7417, https://doi.org/10.1016/j.electacta.2007.06.044.
[67] J. Vila, P. Ginés, J.M. Pico, C. Franjo, E. Jiménez, L.M. Varela, O. Cabeza, Temperature dependence of the electrical conductivity in EMIM-based ionic liquids – evidence of vogel-tamman-fulcher behavior, Fluid Phase Equilib. 242 (2) (2006) 141–146.
[68] J. Pires, L. Timperman, J. Jacquemin, A. Balducci, M. Anouti, Density, conductivity, viscosity, and excess properties of (pyrrolidinium nitrate-based protic ionic liquid plus propylene carbonate) binary mixture, J. Chem. Thermodyn. 59 (2013) 10–19, https://doi.org/10.1016/j.jct.2012.11.020.
[69] S. Bulut, P. Eiden, W. Beichel, J.M. Slattery, T.F. Beyersdorff, T.J.S. Schubert, I. Krossing, Temperature dependence of the viscosity and conductivity of mildly functionalized and non-functionalized [Tf2N](-) ionic liquids, ChemPhysChem 12 (12) (2011) 2296–2310.